

Anatomy of the ATLAS diboson anomaly

B. C. Allanach*

*Department of Applied Mathematics and Theoretical Physics,
Centre for Mathematical Sciences, University of Cambridge, Wilberforce Road, Cambridge, UK*Ben Gripaios[†] and Dave Sutherland[‡]*Cavendish Laboratory, University of Cambridge, J.J. Thomson Ave, Cambridge, UK*

(Dated: September 12, 2018)

We perform a general analysis of new physics interpretations of the recent ATLAS diboson excesses over Standard Model expectations in LHC Run I collisions. Firstly, we estimate a likelihood function in terms of the truth signal in the WW , WZ , and ZZ channels, finding that the maximum has zero events in the WZ channel, though the likelihood is sufficiently flat to allow other scenarios. Secondly, we survey the possible effective field theories containing the Standard Model plus a new resonance that could explain the data, identifying two possibilities, *viz.* a vector that is either a left- or right-handed $SU(2)$ triplet. Finally, we compare these models with other experimental data and determine the parameter regions in which they provide a consistent explanation.

I. INTRODUCTION

The ATLAS experiment has recently reported [1] three excesses in searches based on jet substructure methods for resonances decaying into dibosons (where each jet is interpreted as being a hadronically decaying Z^0 boson or W^\pm boson).

The excesses appear at a diboson invariant mass of around 2 TeV in each of three decay channels studied – WZ , WW , and ZZ – and have local significances of 3.4 , 2.6 , and 2.9σ , respectively and a global significance of 2.5σ in the WZ channel for an integrated luminosity $\mathcal{L} = 20.3 \text{ fb}^{-1}$. ATLAS provided limits upon models that could produce such signals and showed that a 2 TeV W' with weak-boson size gauge coupling or a 2 TeV type I Randall-Sundrum (RS) graviton both have production cross-sections too small to explain the apparent excess [1]. At the same time, CMS finds a global excess of 1.9σ in a boosted search for WH , with the Higgs H decaying hadronically [2] and the W decaying leptonically.

In this note, we explore possible new physics interpretations of the ATLAS excesses. We note that there are other smaller (below 2σ) excesses in other searches for diboson resonances [2–5], but we concentrate here on the ATLAS ones because they are the most statistically significant. We will however, apply constraints from other searches in order to ensure that our new physics explanations are not already excluded. Interpreting the ATLAS excesses in terms of a resonance, data indicate that it is fairly narrow, with a width of less than 100 GeV or so. There have been some recent suggestions for such resonances: for instance, in Ref. [6], walking technicolor was invoked in order to interpret the apparent 2 TeV resonance as a technirho (the discovered Higgs boson is

interpreted as a technidilaton). Several other works concentrate on W' or Z' vector bosons [7–15]. Refs. [16, 17] also have vector resonances motivated by composite dynamics. Ref. [18] postulates a left-right symmetric model to generate the necessary extra bosons.

Here, we pursue a different approach. Rather than examining specific models, we survey the possible models (by which we mean effective field theories, valid at TeV scales) containing the Standard Model (SM) plus a new resonance that can describe the ATLAS anomalies without gross conflict with other data. To do so, we first calculate a likelihood for the truth distribution of events in the WW , WZ , and ZZ channels.¹ Secondly, we use the likelihood analysis and other data to pin down the qualitative features of a possible new physics model. We argue that models based on an $SU(2)_L$ or $SU(2)_R$ triplet vector are most plausible, both of which have already been exploited in specific cases in the literature. However, our approach yields results that are less model dependent.

II. LIKELIHOOD ANALYSIS

The ATLAS diboson search [1] looks for evidence of a heavy resonance which decays to WW , WZ , or ZZ , all of which subsequently decay hadronically. From events containing two fat jets, jet substructure techniques are used to select events wherein each fat jet contains two ‘prongs’ characteristic of a boosted W or Z decay, and thereby also to provide an estimator m_j of the invariant mass of the two subjets within each fat jet. A fat jet is a ‘ W jet’ if $69.4 \text{ GeV} < m_j < 95.4 \text{ GeV}$; it is a ‘ Z jet’ if $79.8 \text{ GeV} < m_j < 105.8 \text{ GeV}$. The three signal regions are then defined as a) WW , containing two W jets; b) WZ , containing a W jet and a Z jet, and c) ZZ , containing two Z jets.

* B.C.Allanach@damtp.cam.ac.uk

† gripaios@hep.phy.cam.ac.uk

‡ dws28@cam.ac.uk

¹ A likelihood analysis was carried out in Ref. [18], but ours differs in several ways.

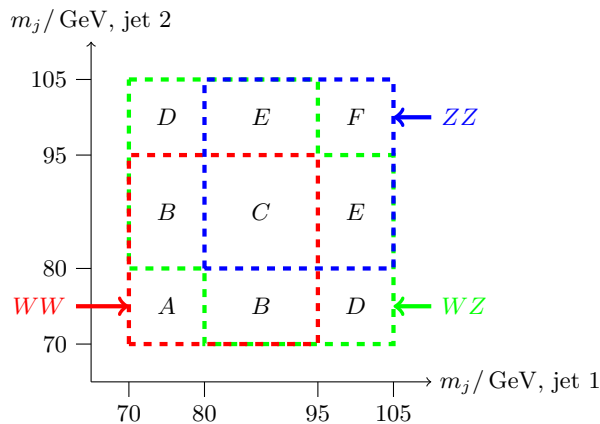


FIG. 1. A simple picture of the WW (red), WZ (green), and ZZ (blue) signal regions used in [1], in the m_j – m_j plane of the two fat jets in an event. We also show our labelling of disjoint signal regions A, B, C, D, E, F .

Additionally, data are reported in the auxiliary information of [1] (<https://twiki.cern.ch/twiki/bin/view/AtlasPublic/ExoticsPublicResults>) for the combinations $WW + ZZ$ and $WW + WZ + ZZ$ of the three aforementioned regions. Clearly, a selected event may be common to more than one signal region — Figure 1 shows a cartoon of the overlap of the signal regions in the (m_j, m_j) plane of the two fat jets.

It is not reported which of the excess events around 2 TeV are common to more than one signal region; however, from the data available, we may infer the number of common excess events as follows. Hereafter, we shall concern ourselves with only the three bins of m_{jj} nearest to 2 TeV, where ATLAS observed the excesses.

Firstly, we seek to disentangle the overlapping signal regions into regions that partition the parameter space of interest. We define six disjoint regions A to F in the (m_j, m_j) plane (Fig. 1) which in combination comprise the five ATLAS signal regions on which we have data:

$$\begin{aligned} WW &= A + B + C, \\ ZZ &= C + E + F, \\ WZ &= B + C + D + E, \\ WW + ZZ &= A + B + C + E + F, \\ WW + WZ + ZZ &= A + B + C + D + E + F. \end{aligned}$$

In Table I we show the three possible arrangements of the events in the disjoint regions A – F that are compatible with the ATLAS data in the five overlapping regions, summed over the three m_{jj} bins of interest. In each of the five signal regions, ATLAS also provides an estimate of the SM background by fitting a smooth curve to the observed m_{jj} spectrum. There is a continuum of possible values for the SM background in the six disjoint regions that are consistent with ATLAS’s numbers in the five overlapping regions — we break the degeneracy by taking the solution with equal ratios of background in A to

	A	B	C	D	E	F
$n_i^{\text{obs},1}$	2	6	5	0	4	0
$n_i^{\text{obs},2}$	1	7	5	0	3	1
$n_i^{\text{obs},3}$	0	8	5	0	2	2
μ_i^{SM}	2.09	2.72	1.00	2.43	0.46	0.34

TABLE I. The three possible arrangements of the observed events into the six disjoint signal regions A – F of Fig. 1, as well as our estimate of the expected event numbers in each region, summed over the three bins $m_{jj}/\text{TeV} \in [1.85 - 1.95, 1.95 - 2.05, 2.05 - 2.15]$.

	W jet tag only	W and Z jet tag	Z jet tag only
true W	0.25	0.36	0.04
true Z	0.11	0.39	0.21

TABLE II. Probability that a W or Z is tagged with a W or Z tag.

F , and in B to E , as is consistent with a QCD dijet background that is roughly flat in the (m_j, m_j) plane. The sums over the three m_{jj} bins of the resulting expected values in the regions A – F are also shown in Table I. Note that the uncertainties in the fitted background spectra are somewhat difficult to take into account since they are likely to be correlated between the different channels, and we do not have access to the correlation matrix. Fortunately, the uncertainties are small and we neglect them.

We now construct our likelihood fit to the LHC production cross section times branching ratios ($\sigma \times \text{BRs}$) of a putative resonance that is responsible for the excess events in Table I. From [1, Fig. 1c], the probabilities that the W or Z from a 2 TeV diboson resonance has an m_j in the W or Z window are approximately as in Table II. Note that these numbers come from the ATLAS simulation of a Randall-Sundrum graviton, which (when it decays to Ws or Zs) decays almost exclusively to longitudinally polarised bosons; transversely polarised bosons would have different m_j distributions [19], so the numbers should be taken *cum grano salis* for other new physics models. The probabilities of a diboson resonance event satisfying the respective m_j cuts of the signal regions A to F are thus shown in Table III, forming a 3 by 6 matrix M_{ji} . We multiply the probabilities in Table III by a factor of $\epsilon = 0.33 \times 0.67$ to match the reported efficiencies of [1, Fig. 2b], with an additional probability of 0.67 for the signal to be in the three m_{jj} bins that we consider [1, Fig. 2a]. Given a vector $s_j = \{s_{WW}, s_{WZ}, s_{ZZ}\}$ of the number of “truth” signal diboson pairs issuing from

M_{ji}	A	B	C	D	E	F
true WW	0.063	0.182	0.132	0.018	0.025	0.001
true WZ	0.028	0.139	0.143	0.057	0.090	0.007
true ZZ	0.012	0.087	0.155	0.047	0.165	0.044

TABLE III. Probability of different diboson candidates from a 2 TeV resonance being tagged in each signal region.

a putative 2 TeV resonance, we expect

$$\mu_i = \mu_i^{SM} + \sum_{j=1}^3 \epsilon b_j s_j M_{ji} \quad (1)$$

events to be tagged in each signal region $i \in \{A, B, C, D, E, F\}$. $b_j = \{0.45, 0.47, 0.49\}$ are the totally hadronic branching fractions of the diboson pairs.

We construct the joint likelihood of tagging n_i events in each of the six signal regions:

$$p(\{n_i\}|\{\mu_i\}) = \prod_{i \in \{A, B, C, D, E, F\}} P(n_i|\mu_i). \quad (2)$$

The six probabilities on the right hand side of Eq. 2 are Poissonian, i.e.

$$P(n|\mu) = \frac{e^{-\mu} \mu^n}{n!}. \quad (3)$$

Substituting Eqs. 1,3 into Eq. 2, we obtain our likelihood

$$p(\{n_i^{\text{obs},\alpha}\} | s_{WW}, s_{WZ}, s_{ZZ}) = \sum_{\alpha=1}^3 \frac{\exp \left[- \sum_{i \in \{A, B, C, D, E, F\}} \left(\mu_i^{SM} + \epsilon \sum_{j=1}^3 b_i s_j M_{ji} \right) \right]}{\prod_{i \in \{A, B, C, D, E, F\}} n_i^{\text{obs},\alpha}!} \times \prod_{i \in \{A, B, C, D, E, F\}} \left(\mu_i^{SM} + \epsilon \sum_{j=1}^3 b_i s_j M_{ji} \right)^{n_i^{\text{obs},\alpha}}, \quad (4)$$

which includes the correlations coming from overlaps in the W and Z tags. We sum over the three independent partitions of events into the regions A to F that are compatible with the ATLAS data, as labelled by α . Eq. 4 allows us to further investigate what the ATLAS fat jet analysis dictates about the different decay channels for a signal. We turn the likelihood into a more familiar value of χ^2 by $\chi^2 = -2 \log p(\{n_i^{\text{obs},\alpha}\} | s_{WW}, s_{WZ}, s_{ZZ})$. Best-fit points will be found by minimising χ^2 (or, equivalently, maximising the likelihood). We shall phrase our results in terms of the production cross section of the 2 TeV resonance X times branching ratio for each decay channel: $\sigma(X) \times BR(X \rightarrow i) = s_j / \mathcal{L}$.

Minimising χ^2 over s_j , we obtain our best-fit point $s_j = \{106, 0, 118\}$, i.e. $\sigma(X^0) \times BR(X^0 \rightarrow W^+W^-) = 5.2$ fb, $\sigma(X^\pm) \times BR(X^\pm \rightarrow W^\pm Z) = 0$ fb, $\sigma(X^0) \times BR(X^0 \rightarrow ZZ) = 5.8$ fb corresponding to expected event numbers $\mu_{WW} = 13.0$, $\mu_{WZ} = 16.1$ and $\mu_{ZZ} = 8.1$ in the three respective ATLAS signal regions WW , WZ , and ZZ . However, as we shall show, the statistical uncertainties are such that sizeable deviations from this best-fit point are possible.

We now examine the constraints upon each channel individually by maximising the p -value over the other two. We show the p -values for each individual channel in Fig. 2. In order to find preferred regions of parameter space, we perform 10^4 pseudoexperiments in order to calculate the p -values, maximising the p -value over any

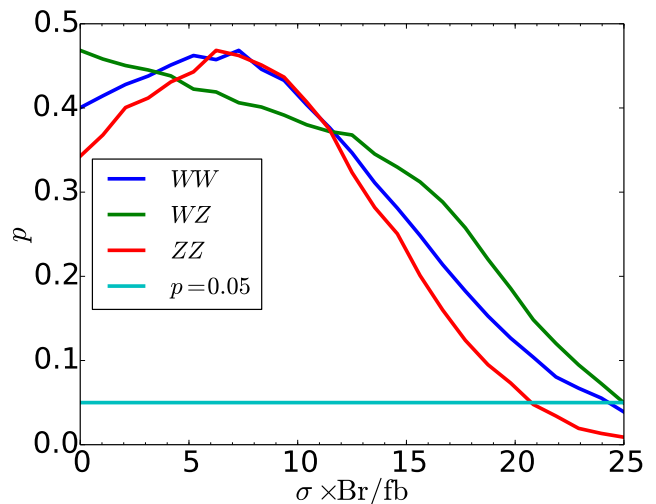


FIG. 2. p -values as a function of production cross section of the 2 TeV resonance X times branching ratio for each decay channel. The p -value has been minimised over the other two signal regions for each line. The horizontal line shows the 95% upper bound. The efficiencies have been unfolded.

	WW	WZ	ZZ
limit/fb	24.3	25.0	20.7

TABLE IV. 95% preferred region upper limits on $\sigma(X) \times BR(X \rightarrow i)$ coming from the ATLAS fat jets analysis (efficiencies have been unfolded).

unseen dimensions. The 95% preferred regions (which all have $p > 0.05$) for each channel are shown in Table IV. We see that each channel has an upper bound of around 20 to 25 fb (equivalent to roughly 400-500 events before efficiencies are taken into account).

Within our approximations, the Standard Model for the joint data set has a p -value of 6×10^{-4} , equivalent to 4.0σ (local significance). This number of sigma would decrease slightly were we to include systematic uncertainties on the backgrounds, but as stated above: these are rather small and so should not cause a large effect. We also obtain a larger local significance than those quoted by ATLAS because we are combining data rather than analysing individual channels.

To get joint constraints upon two of the signal channels, we profile over the unseen one in Fig. 3. The figure shows that whenever one of the channels has a large $\sigma \times BR$ (around 20-25 fb), the anti-correlations imply that the others should be small. The origin is within the 70% CL because the unseen s_j is large there, contributing to each of the tagged channels. For example, the point $s_j = \{254, 0, 0\}$ is the best-fit point with $s_{WZ} = s_{ZZ} = 0$, i.e. $\sigma(X^0) \times BR(X^0 \rightarrow W^+W^-) = 12.9$ fb, $\sigma(X^\pm) \times BR(X^\pm \rightarrow W^\pm Z) = 0$ fb, $\sigma(X^0) \times BR(X^0 \rightarrow ZZ) = 0$ fb, predicting expected numbers of diboson tags including SM background $\mu_{WW} = 15.3$, $\mu_{WZ} = 15.6$, $\mu_{ZZ} = 5.8$, with $\Delta\chi^2 = 3.2$ above the best-fit point. The

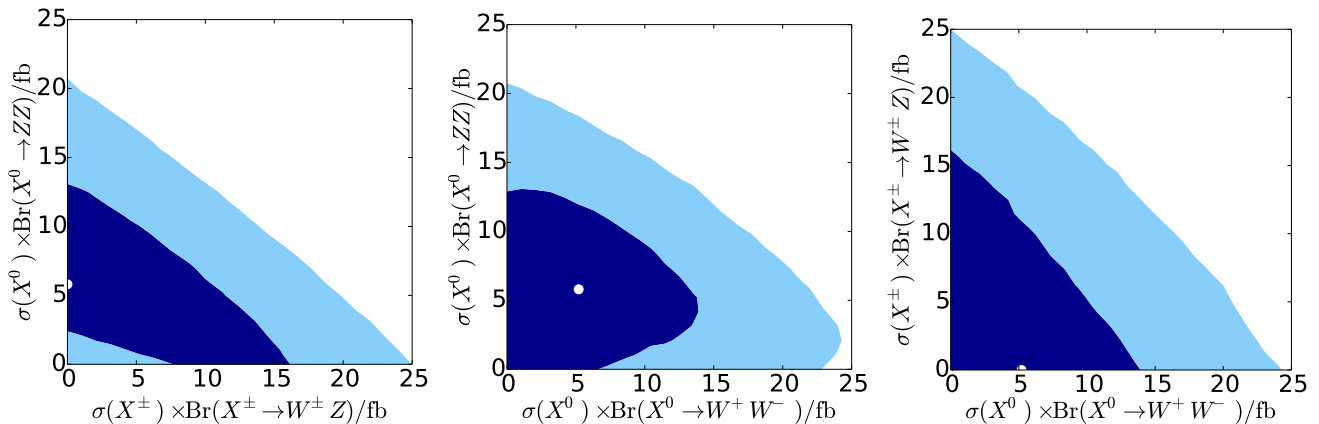


FIG. 3. Joint constraints on the values of $\sigma \times \text{Br}$ for different decay channels of a diboson resonance from the ATLAS fat jets analysis of the Run I LHC before efficiencies. The darkest region corresponds to 70% CL, whereas the next darkest region corresponds to 95% CL. In each panel, the best-fit point is denoted by a white dot.

s_{WW}	s_{WZ}	s_{ZZ}	μ_{WW}	μ_{WZ}	μ_{ZZ}	$\Delta\chi^2$
0	119	86	12.0	16.1	8.2	0.4
106	0	118	13.0	16.2	8.1	0.0
1	223	0	13.0	16.6	7.4	0.8

TABLE V. Best-fit points for the cases where one s_j is set to zero (shown in bold).

unique best-fit point is shown in different projections by the white dots.

If instead we set one of the s_j to zero (which may be predicted by an underlying physical model), we obtain the constraints in Fig. 4. Now, each panel corresponds to a different model hypothesis, and so unlike Fig. 3, the best-fit points (displayed by the white points) are all different. The three best-fit points are displayed in Table V. We see from the table that each fit has $\Delta\chi^2 < 1$, meaning that one cannot significantly discriminate one fit from the other on the basis of ATLAS fat jets data alone. This situation should improve in future analyses exploiting more sophisticated jet substructure methods.

We show the expected jet-jet mass distribution near the 2 TeV signal region in Fig. 5 for the point $s_{WW} = 1$, $s_{WZ} = 223$, $s_{ZZ} = 0$ (this corresponds to $\sigma(X^0) \times \text{Br}(X^0 \rightarrow WW) = 0.05$ fb, $\sigma(X^\pm) \times \text{Br}(X^\pm \rightarrow W^\pm Z) = 11.0$ fb before efficiencies), which is the best-fit point for $s_{ZZ} = 0$: the bottom row of Table V. The figure shows the contamination in the WW and ZZ channels from mis-tagging WZ events. The estimate of the experimental mass resolution on the resonance was based on those of a 2 TeV W' -signal model (whose width is 72 GeV) ATLAS predictions in Ref. [1]. The uncertainties placed on the observed numbers of events are purely statistical (\sqrt{n} for n events), indicating the expected standard deviation of the measurements.

Ref. [18] also performed a likelihood analysis for a resonance decaying into diboson pairs with similar results. There, a selection of ATLAS and CMS diboson searches

are fitted to a wider mass window using a 1.8 TeV resonance rather than a 2 TeV resonance and so quantitative differences are expected, and apparent. We think that it is instructive to examine the constraints from the ATLAS fat jets analysis alone, treating constraints from other diboson analyses separately.

III. NEW PHYSICS DECALOGUE

In order to pare down the possible new physics models explaining the anomaly, we now list a number of qualitative desiderata for such a model.

- (i) The discovery of the Higgs boson and measurement of its couplings (as well as electroweak precision data and flavour physics) all point to physics being described by a theory in which the SM gauge symmetry is spontaneously broken by the SM Higgs at the weak scale. Unlike some predecessors, we thus insist that any model respect the SM gauge symmetry and contain the SM Higgs.
- (ii) The data point to a narrow resonance of high mass (c. 2 TeV). To get a cross-section times branching ratio in the required range then demands sizeable couplings in both production (via quarks or gluons) and decay modes. We therefore insist that these be due to interactions of dimension four or fewer in the lagrangian.
- (iii) Since the final states are bosonic and there is no evidence for the presence of additional invisible particles in the form of missing energy, the resonance should have integral spin j .
- (iv) The requirement of a coupling to gluons or quarks of dimension ≤ 4 implies $j \leq 1$.
- (v) A scalar resonance, ϕ , with $j = 0$ needs electroweak charge in order to couple sizeably to light quarks and provide a production mode. One must ensure both that the scalar does not develop a vacuum ex-

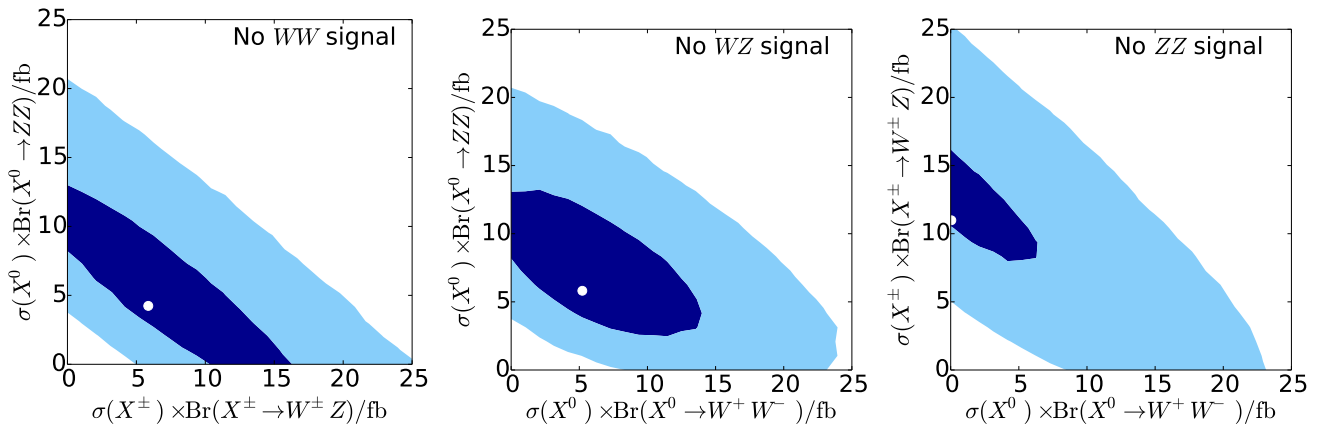


FIG. 4. Joint constraints on the values of $\sigma \times \text{Br}$ for different decay channels of a diboson resonance from the ATLAS fat jets analysis of the Run I LHC, where one of s_{WW} , s_{WZ} or s_{ZZ} is set to zero (i.e. before efficiency corrections). We show the 70% and 95% preferred regions. In each case, the best-fit point is denoted by a white dot.

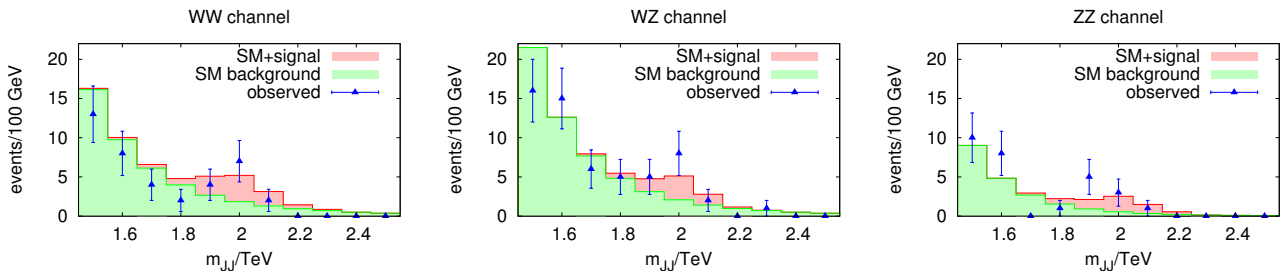


FIG. 5. Invariant mass distribution near the 2 TeV resonance in each channel for $s_{WW} = 1$, $s_{WZ} = 223$, $s_{ZZ} = 0$.

pectation value, which would otherwise, through its Yukawa coupling, change the masses of the light quarks, and also that the scalar mixes with the Higgs, facilitating its decay to dibosons. One cannot satisfy both constraints unless one imposes *ad hoc* relations between different couplings in the Higgs potential. Since we are working the context of generic effective field theories, we wish to avoid such *ad hoc* relations.

- (vi) A consistent effective field theory (EFT) description of a vector resonance ρ^μ , with $j = 1$, requires that it be a (massive) gauge field, so we must enlarge the SM gauge group somehow. If ρ^μ carries electroweak charge, it can couple to both quarks and dibosons (possibly via the Higgs field).
- (vii) We require that the couplings preserve the approximate custodial $SU(2)_L \times SU(2)_R$ symmetry of the SM, both for reasons of economy and because of the stringent constraint coming from the electroweak ρ parameter.² A coupling to quarks then implies that the resonance transforms as either a singlet

or a triplet of either $SU(2)_L$ or $SU(2)_R$. In the singlet case, however, a coupling to dibosons does not result.³ In the triplet cases, couplings of the schematic form (we shall be more precise later) $\rho^\mu H^\dagger D_\mu H$ are allowed, leading to diboson decay modes.

- (viii) A coupling to quarks also yields corrections to electroweak precision data that are non-universal, in general. At least in the universal limit, with couplings $\lesssim O(1)$, we get tree-level contributions to the S parameter (which typically provides one of the strongest constraints) that are acceptably small.
- (ix) Sizeable non-universal couplings to quarks also lead to corrections to the decay rate of the Z boson to hadrons and to the unitarity of the CKM matrix. Such couplings are much less constrained if they are to right-handed quarks [20], favouring the model with a right-handed triplet. One can even exploit symmetries to forbid tree-level contributions in this case [21].

² It is possible that the couplings required to reproduce the excesses are small enough that this requirement can be relaxed.

To study this requires a detailed electroweak fit for such models, which we leave to future work.

³ If we allow for custodial symmetry violation, the singlet can couple to WW .

(*x*) In order to avoid problems with flavour physics constraints, and for simplicity's sake, we assume that the resonance couples in a flavour-diagonal way to the two light quark generations only.⁴

We have thus honed in on a pair of possible models, with either a new $SU(2)_L$ or $SU(2)_R$ triplet resonance with sizeable couplings to the Higgs field and light quarks. We now build the most general EFTs and show that the anomalies can be explained without contradicting limits on new physics from other experiments.

IV. EFTS AND THEIR FIT TO DATA

In this section we write down the most general EFTs satisfying the conditions of §III (using the rules of [22, 23]) and briefly describe their phenomenology. For each model we find the parameters that best fit the ATLAS diboson excess.

A. Left handed triplet model

Adding a zero-hypercharge heavy vector $SU(2)_L$ triplet ρ_μ^a (indexed by $a \in \{1, 2, 3\}$ and comprising three charge eigenstates ρ^+ , ρ^0 and ρ^-) to the SM results in the most general lagrangian up to dimension four of

$$\begin{aligned} \mathcal{L} = \mathcal{L}_{\text{SM}} &- \frac{1}{4}\rho_{\mu\nu}^a\rho^{a\mu\nu} + \left(\frac{1}{2}m_\rho^2 + \frac{1}{4}g_m^2 H^\dagger H\right)\rho_\mu^a\rho^{a\mu} \\ &- 2g\epsilon^{abc}\partial_{[\mu}\rho_{\nu]}^a W^{b\mu} \rho^{c\nu} - g\epsilon^{abc}\partial_{[\mu}W_{\nu]}^a \rho^{b\mu} \rho^{c\nu} \\ &+ \left(\frac{1}{2}ig_\rho\rho_\mu^a H^\dagger \sigma^a D^\mu H + \text{h.c.}\right) + g_q\rho_\mu^a \bar{Q}_L \gamma^\mu \sigma^a Q_L \\ &+ g_l\rho_\mu^a \bar{L}_L \sigma^a \gamma^\mu L_L + \dots, \end{aligned}$$

where σ^a are the Pauli matrices, g is the $SU(2)_L$ gauge coupling and $\partial_{[\mu}\rho_{\nu]}^a \equiv \frac{1}{2}(\partial_\mu\rho_\nu^a - \partial_\nu\rho_\mu^a)$.⁵ The coefficient of the term $- \epsilon^{abc}\partial_{[\mu}W_{\nu]}^a \rho^{b\mu} \rho^{c\nu}$ is set to g because such a value results in a higher ultra-violet cut-off scale Λ , where Λ is associated with unitarity violation. However, one could also consider small deviations from g of order $g m_\rho^2/\Lambda^2$: these must not be large otherwise the régime of validity of our EFT is compromised. There are additional terms that we have not written, such as $\rho^2 W^2$, that do not affect the discussion here, but which restore $SU(2)_L$ gauge invariance and may be relevant for future searches. The ' $\rho H^\dagger D H$ ' coupling, after electroweak symmetry breaking (EWSB), mixes the ρ^\pm with the W^\pm , and the ρ^0 with the Z , with mixing angle of order $\frac{gg_\rho v^2}{4m_\rho^2}$ for Higgs vacuum expectation value $v = 246$ GeV, analogously to the rho meson in hadronic physics. The same

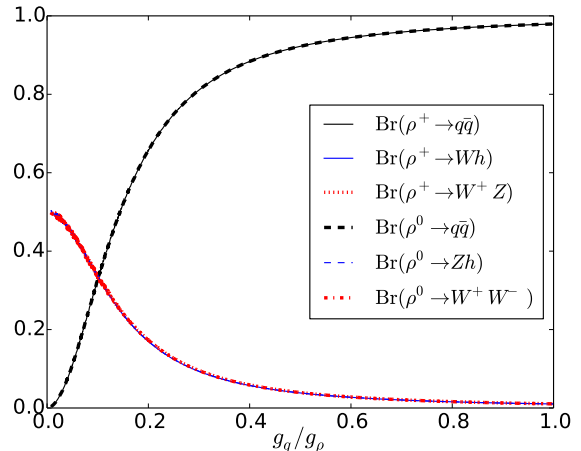


FIG. 6. The branching ratios of the ρ^+ and ρ^0 of the left handed triplet model, as a function of their coupling to quarks g_q over their coupling to bosons g_ρ . Note the equal branching ratios to Wh and WZ , and also to Zh and WW , as predicted by [17]. The dijet branching ratios of the ρ^+ and ρ^0 overlap (black curves), as do their diboson branching ratios (blue and red curves).

operator mediates the decay of the ρ^0 to W^+W^- and Zh , and that of the ρ^\pm to $W^\pm Z$ and $W^\pm h$.

As described above, we assume the ρ only couples to the first two quark generations, with equal strength; we also set $g_l = 0$, given the absence of a 2 TeV bump in dilepton searches [25, 26]. We assume for simplicity that $g_m = 0$; for example a $g_m = 4$ would only increase the partial width of the ρ s to either Wh or Zh by $\sim 10\%$. We use FeynRules 2.0.6 [27] and MadGraph5_aMC@NLO v2.2.3 [28] to simulate the production and decay of the ρ s at leading order, using a K factor of 1.3 consistent with that of Drell-Yan W^\pm production [29]. The number of produced ρ s are then multiplied by their branching ratios to dibosons (Fig. 6), the efficiencies in Table III and the overall efficiency factor of ϵ to obtain a prediction for the number of signal events in the six disjoint regions A to F , as a function of the lagrangian parameters. Using the observations of Table I, we perform pseudoexperiments to obtain a p value for each set of parameters; Fig. 7 shows the resulting good-fit regions in the (g_ρ, g_q) plane. Towards the top of the best fit region the ρ s are produced copiously but rarely decay to dibosons, whereas towards the right the ρ s are produced rarely but almost always decay to dibosons (where ‘dibosons’ includes the decays to Wh or Zh). We also overlay in Fig. 7 the 95% CL limits on $\sigma \times \text{Br}(W' \rightarrow WZ)$ from other searches for diboson resonances, namely the CMS all hadronic search [5] (12 fb) and the ATLAS semileptonic search [30] (20 fb). Note that we do not consider the CMS semileptonic search, because the only readily available limits are for a type I RS graviton, which has considerably higher acceptances than, say, a W' . Given the similarity of the ATLAS and CMS semileptonic limits on the type I RS

⁴ It is likely that this requirement can also be relaxed somewhat.

⁵ A similar lagrangian was considered in Ref. [24].

graviton, we assume any recasting of the CMS search onto the triplet model of this section would yield limits comparable to the ATLAS W' limit displayed in Fig. 7.

Also shown in Fig. 7 is the CMS 95% CL limit on $\sigma(X) \times \text{Br}(X \rightarrow Wh, Zh) = 8 \text{ fb}$ for a 2 TeV spin one resonance X [31]. The limit is quite constraining for the $SU(2)_L$ triplet, given the roughly equal branching ratio of the ρ^\pm to WZ and Wh , as well as that of the ρ^0 to WW and Zh . Interestingly, the analogous limit for a marginally lighter 1.8 TeV resonance is much weaker (14 fb).

We now comment on the compatibility with electroweak precision constraints.⁶ The model is non-universal, but we can estimate the constraints by assuming that ρ couples equally to all 3 quark generations, such that we may compare with the analysis performed using a flavour-symmetric basis of dimension-six SM operators in [34]. Integrating out the ρ , we obtain 3 such operators: $\frac{g_\rho^2}{4m_\rho^2}(iH^\dagger\sigma^a\overleftrightarrow{D}_\mu H)(iH^\dagger\sigma^a\overleftrightarrow{D}^\mu H)$, $\frac{g_\rho g_q}{2m_\rho^2}\mathcal{O}_L^{(3)q} \equiv \frac{g_\rho g_q}{2m_\rho^2}(iH^\dagger\sigma^a\overleftrightarrow{D}_\mu H)(\overline{Q}_L\sigma^a\gamma^\mu Q_L)$, and $\frac{g_q^2}{m_\rho^2}(\overline{Q}_L\sigma^a\gamma_\mu Q_L)(\overline{Q}_L\sigma^a\gamma^\mu Q_L)$. Re-writing these in the basis of [35], we find that only $\mathcal{O}_L^{(3)q}$, contributes to Z pole measurements. We use the 95% CL limit on its Wilson coefficient alone, given in Eq. (19) of [34], to place the approximate bound $|g_\rho g_q| \lesssim 0.5$, which is compatible with the values required to fit the excess in the ATLAS diboson search (see the grey dashed line in Fig. 7).

The ρ boson necessarily couples to quarks (in order to obtain the production cross-section), and so we should consider constraints coming from resonance searches to dijets at an invariant mass of 2 TeV. CMS, for instance, places a 95%CL upper limit of 60 fb [36] for $\sigma \times BR(\rho \rightarrow q\bar{q}) \times A$, where $A \leq 1$ is acceptance (ATLAS' analogous upper bound is 110 fb [37]). Assuming an acceptance $A \sim 0.6$, as quoted in [36] for isotropic decays, the CMS limit rules out the otherwise good fit points with large $BR(\rho \rightarrow q\bar{q})$, as shown in Fig. 7, preferring instead a sizeable branching ratio of the ρ to dibosons.

B. Right handed triplet model

Applying the same logic as in section IV A, the most general lagrangian up to dimension four containing an

⁶ Electroweak fits to similar were performed in [32, 33], but do not lead to significant constraints on the models considered here.

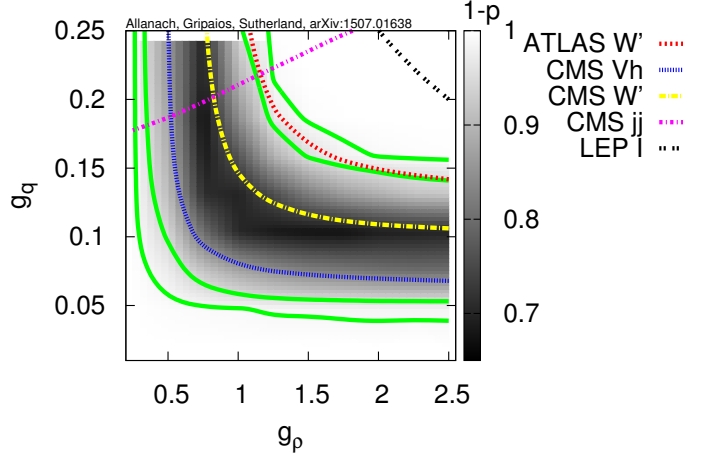


FIG. 7. Preferred regions in the plane of the $SU(2)_L$ triplet's coupling to bosons, g_ρ , and quarks, g_q , as determined from the number of events observed in the six disjoint signal regions (see Table I). We show the 95%, 99% preferred regions by the inner and outer pair of solid lines, respectively. Also shown are the 95% CL limits on a W' model from [30] (ATLAS W') and [5] (CMS W') which should be similar to the limits on the $SU(2)_L$ triplet considered here, the limit from the CMS search for resonances decaying to $Wh, Zh \rightarrow qq\bar{b}\bar{b}$ [31] ('CMS Vh'), and the limit from the CMS dijet resonance search [36] ('CMS jj'). The line denoted 'LEP I' depicts the approximate constraint from electroweak precision tests at LEP I. The region above each broken line is excluded.

additional triplet of $SU(2)_R$, ρ_μ^a , is⁷

$$\begin{aligned} \mathcal{L} = & \mathcal{L}_{\text{SM}} - \frac{1}{4}\rho_{\mu\nu}^a\rho^{a\mu\nu} + \left(\frac{1}{2}m_\rho^2 + \frac{1}{4}g_m^2 H^\dagger H\right)\rho_\mu^a\rho^{a\mu} \\ & - 2g'\epsilon^{ab3}\partial_{[\mu}\rho_{\nu]}^a\rho^{b\mu}B^\nu - g'\epsilon^{3bc}\partial_{[\mu}B_{\nu]}c\rho^{b\mu}\rho^{c\nu} \\ & + \left(-\frac{1}{4}ig_\rho\rho_\mu^a\text{Tr}(\Pi\sigma^a D^\mu\Pi^\dagger) + \text{h.c.}\right) + g_q\rho_\mu^a\overline{Q}_R\gamma^\mu\sigma^a Q_R, \end{aligned}$$

where $Q_R = \begin{pmatrix} u_R \\ d_R \end{pmatrix}$, g' is the $U(1)_Y$ gauge coupling, and we have taken advantage of notation in which the $SU(2)_L \times SU(2)_R$ symmetry of the Higgs doublet $H = \begin{pmatrix} \phi^+ \\ \phi^0 \end{pmatrix}$ is manifest, defining $\Pi = (H, H^c) = \begin{pmatrix} \phi^+ & \overline{\phi^0} \\ \phi^0 & -\phi^- \end{pmatrix}$ and $D_\mu\Pi = \partial_\mu\Pi + \frac{1}{2}igW_\mu^a\sigma^a\Pi + \frac{1}{2}ig'B_\mu\Pi\sigma^3$. Much the same phenomenology results as in the left handed triplet case: the charged and neutral components of the ρ mix to the same degrees with the W s and Z respectively (after EWSB); they can also decay to WZ/Wh , or WW/Zh , respectively.

The branching ratios of the ρ s are identical to those of the left-handed triplet model, shown in Fig. 6. An identical analysis to §IV A yields Fig. 8, showing the points in

⁷ We have neglected a small mass splitting, of $O(\frac{g'^2}{g^2})$, in m_ρ .

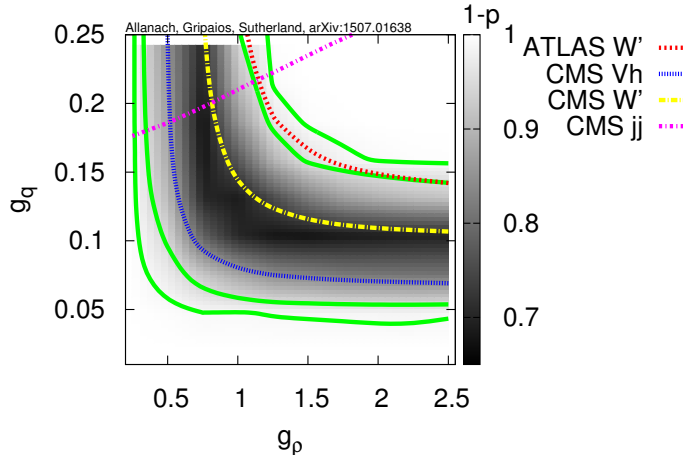


FIG. 8. Preferred regions in the plane of the $SU(2)_R$ triplet's coupling to bosons, g_ρ , and quarks, g_q . We show the 95%, 99% preferred regions by the inner and outer pair of solid lines, respectively. Also shown are the 95% CL limits on a W' model from [5] (ATLAS W') and [30] (CMS W') which should be similar to the limits on the $SU(2)_R$ triplet considered here, the limit from the CMS search for resonances decaying to $Wh, Zh \rightarrow qq\bar{b}\bar{b}$ [31] ('CMS Vh '), and the limit from the CMS dijet resonance search [36] ('CMS jj '). The region above each broken line is excluded.

the (g_ρ, g_q) plane that best fit the ATLAS diboson excess, along with relevant constraints from other diboson resonance searches. A comparison with Fig. 7 shows that the fit to the diboson anomaly is practically identical to the $SU(2)_L$ triplet. The other constraints are also identical, except for the EWPT.

Unfortunately, we cannot perform a robust fit to EWPT using [34] in this case, because integrating out the ρ generates operators such as $(i\vec{H}^\dagger \overleftrightarrow{D}_\mu H)(\overline{u_R} \gamma^\mu d_R)$ that are not considered there. So a detailed fit *ab initio*

is required, which we leave for future work. As we argued above, the constraints will be much weaker in this case, because contributions to hadronic decays of the Z are suppressed (typically by an order of magnitude [20, 34]) and because CKM unitarity violation is absent. We thus expect that there will be no significant constraint on the region of allowed couplings.

V. CONCLUSIONS

Figs. 7 and 8 show that right- or left- handed triplets can explain the ATLAS diboson excesses without contradicting other constraints. Our effective field theory analysis should be less model dependent than specific models that have recently appeared in the literature. Indeed, we provide general likelihood constraints on a resonance which can decay via channels WW, WZ and ZZ in Figs. 3,4. The production cross sections of both the $SU(2)_L$ and $SU(2)_R$ triplets increase by a factor of 7 in 13 TeV collisions (relevant for Run II of the LHC), compared to those at 8 TeV on which the ATLAS fat-jets diboson resonance search was based. By the end of 2015, the models considered would conservatively predict at least as many signal events as in previous run, which would be observed foremost in the WZ and Wh all-hadronic channels. The channels where the W s and Z s decay leptonically are presently a factor of ~ 2 less sensitive; this may improve if the efficiency of jet substructure methods worsens due to higher pileup.

ACKNOWLEDGEMENTS

This work has been partially supported by STFC grant ST/L000385/1. We thank M. Redi, J. Tattersall, J. Thaler, A. Wulzer and members of the Cambridge SUSY Working Group for discussions. BG acknowledges MIAPP and King's College, Cambridge. DS acknowledges the support of Emmanuel College, Cambridge.

-
- [1] G. Aad et al. (ATLAS) (2015), 1506.00962.
 - [2] Tech. Rep. CMS-PAS-EXO-14-010, CERN, Geneva (2015), URL <http://cds.cern.ch/record/2002903>.
 - [3] V. Khachatryan et al. (CMS), JHEP **1408**, 174 (2014), 1405.3447.
 - [4] G. Aad et al. (ATLAS), Eur.Phys.J. **C75**, 209 (2015), 1503.04677.
 - [5] V. Khachatryan et al. (CMS), JHEP **1408**, 173 (2014), 1405.1994.
 - [6] H. S. Fukano, M. Kurachi, S. Matsuzaki, K. Terashi, and K. Yamawaki (2015), 1506.03751.
 - [7] A. Alves, A. Berlin, S. Profumo, and F. S. Queiroz (2015), 1506.06767.
 - [8] J. Hisano, N. Nagata, and Y. Omura (2015), 1506.03931.
 - [9] K. Cheung, W.-Y. Keung, P.-Y. Tseng, and T.-C. Yuan (2015), 1506.06064.
 - [10] S.-S. Xue (2015), 1506.05994.
 - [11] B. A. Dobrescu and Z. Liu (2015), 1506.06736.
 - [12] J. Aguilar-Saavedra (2015), 1506.06739.
 - [13] Y. Gao, T. Ghosh, K. Sinha, and J.-H. Yu (2015), 1506.07511.
 - [14] Q.-H. Cao, B. Yan, and D.-M. Zhang (2015), 1507.00268.
 - [15] G. Cacciapaglia and M. T. Frandsen (2015), 1507.00900.
 - [16] D. B. Franzosi, M. T. Frandsen, and F. Sannino (2015), 1506.04392.
 - [17] A. Thamm, R. Torre, and A. Wulzer (2015), 1506.08688.
 - [18] J. Brehmer, J. Hewett, J. Kopp, T. Rizzo, and J. Tattersall (2015), 1507.00013.

- [19] Tech. Rep. CMS-PAS-JME-13-006, CERN, Geneva (2013), URL <http://cds.cern.ch/record/1577417>.
- [20] M. Redi and A. Weiler, *JHEP* **1111**, 108 (2011), 1106.6357.
- [21] K. Agashe, R. Contino, L. Da Rold, and A. Pomarol, *Phys.Lett.* **B641**, 62 (2006), hep-ph/0605341.
- [22] S. R. Coleman, J. Wess, and B. Zumino, *Phys.Rev.* **177**, 2239 (1969).
- [23] J. Callan, Curtis G., S. R. Coleman, J. Wess, and B. Zumino, *Phys.Rev.* **177**, 2247 (1969).
- [24] A. R. Zerwekh, *Eur.Phys.J.* **C46**, 791 (2006), hep-ph/0512261.
- [25] V. Khachatryan et al. (CMS), *JHEP* **1504**, 025 (2015), 1412.6302.
- [26] G. Aad et al. (ATLAS), *Phys.Rev.* **D90**, 052005 (2014), 1405.4123.
- [27] A. Alloul, N. D. Christensen, C. Degrande, C. Duhr, and B. Fuks, *Comput.Phys.Commun.* **185**, 2250 (2014), 1310.1921.
- [28] J. Alwall, R. Frederix, S. Frixione, V. Hirschi, F. Maltoni, et al., *JHEP* **1407**, 079 (2014), 1405.0301.
- [29] C. Anastasiou, L. J. Dixon, K. Melnikov, and F. Petriello, *Phys.Rev.* **D69**, 094008 (2004), hep-ph/0312266.
- [30] G. Aad et al. (ATLAS), *Eur.Phys.J.* **C75**, 69 (2015), 1409.6190.
- [31] V. Khachatryan et al. (CMS) (2015), 1506.01443.
- [32] F. del Aguila, J. de Blas, and M. Perez-Victoria, *JHEP* **1009**, 033 (2010), 1005.3998.
- [33] J. de Blas, J. Lizana, and M. Perez-Victoria, *JHEP* **1301**, 166 (2013), 1211.2229.
- [34] A. Pomarol and F. Riva, *JHEP* **1401**, 151 (2014), 1308.2803.
- [35] J. Elias-Miro, J. Espinosa, E. Masso, and A. Pomarol, *JHEP* **1311**, 066 (2013), 1308.1879.
- [36] V. Khachatryan et al. (CMS), *Phys. Rev.* **D91**, 052009 (2015), 1501.04198.
- [37] G. Aad et al. (ATLAS), *Phys.Rev.* **D91**, 052007 (2015), 1407.1376.